V. MICROWAVE ELECTRONICS*

Prof. L. D. Smullin
Prof. H. A. Haus
Prof. S. Saito (visiting fellow)
A. Bers
R. M. Bevensee
T. J. Connor
B. W. Faughnan
C. Fried
B. A. Highstrete
A. J. Lichtenberg
E. V. Sorensen

A. NOISE

1. Minimum Noise Figure of Traveling-Wave Amplifiers

The one-dimensional, single-mode theory of noise in beams at microwave frequencies predicts a minimum noise figure for traveling-wave amplifiers that is given (1) by the expression

$$F_{min} = 1 + J(S-\Pi) \tag{1}$$

where

$$J = \frac{4\pi}{kT}(4QC\, f_{max}\, f_{min})^{1/2} \tag{2}$$

$$S = \left| \frac{e}{\pi} \frac{\lambda_e}{\lambda_q} V_o\, 10^{W_1/10} \right| \quad \text{(joules)} \tag{3}$$

The quantities f_{max} and f_{min} are the largest and smallest values of the f-function, which was first defined by Watkins (2); T is the ambient temperature in degrees absolute; k is Boltzmann's constant; QC, Pierce's space-charge parameter (3); λ_q, the reduced plasma wavelength; V_o, the beam voltage; e, the electron charge. The electronic wavelength λ_e is given as

$$\lambda_e = 2\pi v_o/\omega \tag{4}$$

where v_o is the drift velocity, and ω is the frequency which is of interest. W_1 is the average of the noise standing wave in the drift region, in decibels with respect to shot noise. The quantity Π is a measure of the correlation between current and velocity fluctuations in the beam. By use of this equation, it is possible to determine experimentally whether or not correlation exists. Thus we rewrite Eq. 1 in the form

$$\frac{\Pi}{S} = 1 - \frac{F_{min} - 1}{JS} \tag{5}$$

Π/S can assume values between +1 and −1, where a value of zero corresponds to a condition of no correlation.

The aforementioned theory also predicts the noise standing-wave ratio and helix position that are necessary to achieve minimum noise figure. These values are given as

* This work was supported in part by Purchase Order DDL-B158.

$$\rho^2_{opt} = \frac{\Psi_{max}}{\Psi_{min}} = \frac{f_{max}}{f_{min}} \tag{6}$$

$$\theta_{opt} = \frac{\pi}{2} + \theta_o \tag{7}$$

where θ_o is the angle from the helix entrance to the closest maximum of the f-function. Ψ represents the noise power in the drift region, attributed to current fluctuations in the beam. If Eqs. 6 and 7 agree with the experiment, then Eq. 5 can be assumed to be applicable.

a. Experimental results

This experiment was performed on three RCA low-noise guns, in a demountable vacuum system. The helix that was used had an inside diameter of 0.096 inch. The cavity used to measure W_1 resonated at 2930 mc. Figures V-1, V-2, and V-3 are the noise curves of the guns for the conditions that give minimum noise figure. The experimental and calculated results are summarized in Table V-1. The first minimum and maximum were used in each case to determine W_1 and ρ^2_{opt}. The quantities J, θ_{opt} theoretical, and ρ^2_{opt} theoretical were found from the curves of references 2 and 4. All experimental results were obtained 2.5 to 7 hours after activation.

Table V-1

	Gun A	Gun B	Gun C
λ_e/λ_q	0.0193	0.0195	0.0185
QC	0.39	0.41	0.42
d	0.1	0.1	0.1
ρ^2_{opt} (theoretical)	2.6	2.55	2.5
ρ^2_{opt} (experimental)	2.75	2.10	2.4
θ_{opt} (theoretical)	-38°	-38°	-38°
θ_{opt} (experimental)	-46°	-58°	-41°
J $(\text{joules})^{-1}$	1.76×10^{21}	1.75×10^{21}	1.76×10^{21}
W_1 (db)	-19.2	-17.0	-18.1
S (joules)	5.91×10^{-21}	10.05×10^{-21}	7.24×10^{-21}
F_{min} (db)	8.1	9.2	10.2
Π/S	+0.48	+0.58	+0.26
Probable error $\Delta\left(\frac{\Pi}{S}\right)$	±0.15	±0.12	±0.26

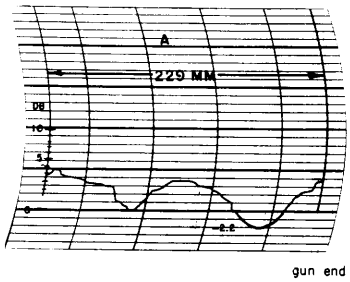

Fig. V-1. Noise curve — Gun A, 0.040-inch oxide-coated cathode;

W_1 = −19.2 db	V_1 = 0 volt	V_{heat} = 3 volts
I_o = 322 μa	V_2 = 30 volts	B = 955 gauss
I_i = 3 μa	V_3 = 82 volts	P = 5×10^{-7} mm Hg
V_o = 496 volts	I_{heat} = 0.91 amp	T_{room} = 31.8°C

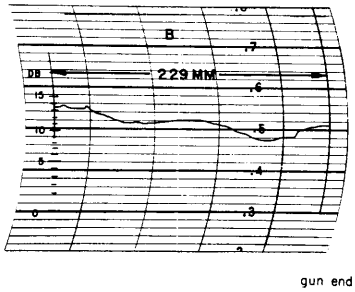

Fig. V-2. Noise curve — Gun B, 0.040-inch oxide-coated cathode;

W_1 = −17.0 db	V_1 = 0 volt	V_{heat} = 3 volts
I_o = 314 μa	V_2 = 25.3 volts	B = 930 gauss
I_i = 2.8 μa	V_3 = 70 volts	P = 8.5×10^{-7} mm Hg
V_o = 499 volts	I_{heat} = 0.91 amp	T_{room} = 33°C

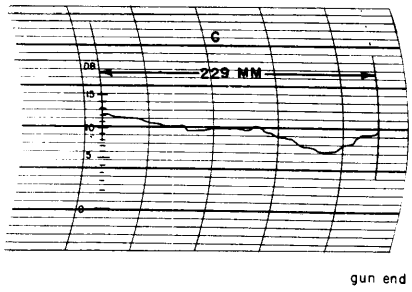

Fig. V-3. Noise curve — Gun C, 0.040-inch oxide-coated cathode;

W_1 = −18.1 db	V_1 = 0 volt	V_{heat} = 3 volts
I_o = 304 μa	V_2 = 28 volts	B = 955 gauss
I_i = 2.6 μa	V_3 = 80 volts	P = 7.5×10^{-7} mm Hg
V_o = 493 volts	I_{heat} = 0.92 amp	T_{room} = 31°C

b. Conclusions

The increasing noisiness of the curves, which is not predicted by theory, is not understood at the present time. Calculations indicate that interception current and electron-gas collisions are probably not the cause.

In spite of these anomalous effects, the theory does closely predict the conditions for minimum noise figure, indicating that the excess noise is not pronounced at the helix beginning, where the noise figure is primarily set up. Thus, since Eqs. 6 and 7 are applicable, Eq. 5 is probably applicable too.

Presuming, then, that Eq. 5 can be used, we conclude that, within the range of probable error, there is evidence of positive correlation in all of the guns that were tested. The results of this experiment are presented in more detail in reference 5.

T. J. Connor

References

1. H. A. Haus, J. Appl. Phys. 26, 560 (1955).
2. D. A. Watkins, Technical Report 31, Electronics Research Laboratory, Stanford University, March 15, 1951.
3. J. R. Pierce, Traveling-Wave Tubes (D. Van Nostrand Company, Inc., New York, 1950).
4. J. R. Pierce and W. E. Danielson, J. Appl. Phys. 25, 1163 (1954).
5. T. J. Connor, S. M. Thesis, Department of Electrical Engineering, M.I.T., 1956.

Note added in proof: The results reported above still appear to be in contradiction to those obtained at the RCA Laboratories, Princeton, N. J. (See the following table.) Aside from the fact that our data indicate $\Pi/S > 0$, and the RCA data make $\Pi/S \approx 0$, the

	MIT			RCA[1,2]	
Gun	A	B	C	1	2
$S \times 10^{21}$ (joules)	5.9	10	7.2	4.8	4.8
F_{min} (ratio)	6.5	8.3	10.5	12.6	10.8
Π/S	$+0.48 \pm .15$	$+0.58 \pm .12$	$+0.26 \pm .23$	$0 \pm .3$	0

differences lie in the higher value of S and the low noise figures in the M.I.T. measurements. Whether these differences are real or experimental remains to be determined.

L. D. Smullin

References

1. Fourth Quarterly Report, Research and development on microwave generators, mixing devices and amplifiers, David Sarnoff Research Center, RCA Laboratories Division, Princeton, N. J., Oct. 31, 1955.
2. Ibid., Seventh Quarterly Report, Aug. 1, 1956.

B. HIGH-POWER MICROWAVE TUBES*

1. Multicavity Klystrons

In the Quarterly Progress Report of April 15, 1956, page 25, we presented a small-signal analysis for multicavity klystrons in which all cavities are identical, tuned synchronously, and spaced equidistantly along the electron beam. It was shown that a two-wave theory predicts very high gain for tubes with a large number of cavities.

When considering bandpass characteristics of multicavity klystrons the structure must be allowed to assume a more general form. The cavities will, in general, be detuned with respect to a center frequency, will possibly have different Q's, and may not be spaced equidistantly. The multicavity klystron gain must now be written in such a form that it shows explicitly the effect of each cavity and drift.

The interaction region of a multicavity klystron can, in general, be divided into three parts (see Fig. V-4): (a) the input cavity, which is fed by the signal source and impresses a (kinetic) voltage V upon the beam; (b) the output cavity, which is excited by the current modulation I in the beam and delivers the amplified signal to the load; and (c) the intermediate interaction space, which is uncoupled to both input and output cavities. The gain (actual power out divided by available power in) is

$$\mathcal{G} = 4 \frac{M^4 G_{in} G_L}{|Y_{in} Y_{out}|^2} \left| \frac{I}{V} \right|^2 \qquad (1)$$

where $G_{in} = G_s + G_{el}$ of the input cavity, Y_{in} is the gap admittance of the input cavity, and Y_{out} is the gap admittance of the output gap. Hence the gain is proportional to I/V,

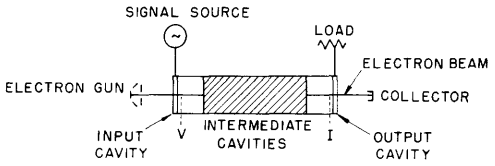

Fig. V-4. Multicavity klystron structure.

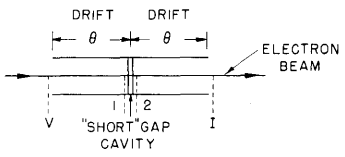

Fig. V-5. Simple multicavity klystron interaction structure.

* This work was sponsored in part by the Office of Naval Research under contract Nonr 1841(05).

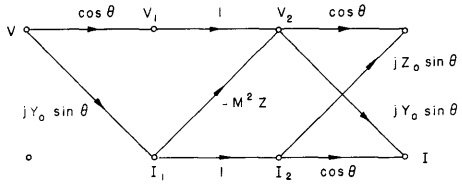

Fig. V-6. Signal flow graph for structure of Fig. V-5. $Y_o = 1/Z_o$ is the characteristic impedance of the drift.

$$\left(\frac{I}{V}\right)_c = (j\,Y_o \sin\theta)(-M^2 Z)(j\,Y_o \sin\theta)$$

$$= Y_o^2 \sin^2\theta\, M^2 Z$$

$$\left(\frac{I}{V}\right)_f = j\,Y_o \sin 2\theta$$

Fig. V-7. The two basic gain mechanisms.

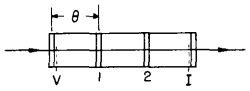

$$\frac{I}{V} = -j\,Y_o^3 \sin^3\theta\, z_1 z_2 + Y_o^2 \sin\theta \sin 2\theta\,(z_1 + z_2) + j\,Y_o \sin 3\theta$$

Fig. V-8. I/V for a four-cavity klystron with equidistant spacing between cavities. The characteristic impedance of the drift is Y_o; $z = M^2 Z$.

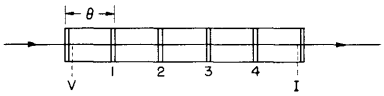

$$\frac{I}{V} = j\,Y_o^5 \sin^5\theta\, z_1 z_2 z_3 z_4 - Y_o^4 \sin^3\theta \sin 2\theta\,(z_1 z_2 z_3 + z_1 z_2 z_4 + z_1 z_3 z_4 + z_2 z_3 z_4) - j\,Y_o^3 \sin^2\theta \sin 3\theta\,(z_1 z_2 + z_1 z_4 + z_3 z_4) - j\,Y_o^3 \sin^2\theta \sin\theta\,(z_1 z_3 + z_2 z_4 + z_2 z_3) + Y_o^2 \sin\theta \sin 4\theta\,(z_1 + z_4) + Y_o^2 \sin 2\theta \sin 3\theta\,(z_2 + z_3) + j\,Y_o \sin 5\theta$$

Fig. V-9. I/V for a six-cavity klystron with equidistant spacing between cavities.

which characterizes the intermediate cavities. It is this quantity that we shall use in describing the gain behavior of the multicavity klystron.

In order to determine I/V for an arbitrary multicavity klystron intermediate structure, it is useful to recognize that under small-signal operation superposition applies. Consider the simple structure shown in Fig. V-5. Assuming that the electron beam enters with a voltage V, we wish to find the current I at the output. The usual technique would involve combining the matrix relations for the drift region and cavity gap and solving for I/V. We shall illustrate this process with the aid of S. J. Mason's flow-graph technique. Figure V-6 gives the signal flow graph for our structure. The desired result is

$$\frac{I}{V} = Y_o^2 \sin^2\theta\, M^2 Z + \cos\theta\, j\, Y_o \sin\theta + j\, Y_o \sin\theta \cos\theta$$

$$= Y_o^2 \sin^2\theta\, M^2 Z + j\, Y_o \sin 2\theta \qquad (2)$$

From the second equation in Eqs. 2, we recognize, however, that the two terms actually represent two, physically distinct, types of gain. The first term represents a "cascade" type of gain (Fig. V-7); that is, by drifting, V produces I_1, which flows through the gap and thus impresses V_2 upon the beam, which then drifts to produce I. The second term is a "feedforward" type of gain; that is, V drifts through 2θ, ignoring the cavity, and produces I. This latter type of gain exists because of current continuity at a short gap. The over-all I/V is, by superposition, equal to the sum of these two terms.

Once we recognize the existence of this superposition technique, we can write I/V by inspection without recourse to tedious matrix manipulations or even to flow graphs. It also follows that I/V for any multicavity klystron can be written by inspection with the use of our superposition technique. Figure V-8 gives an example of the I/V for a four-cavity klystron. The first term is the cascade term for both cavities; the second term is obtained by feedforward over one cavity at a time; and the last term is a feedforward over two cavities at a time — simply a drift of 3θ. A more complex example, a six-cavity klystron, is shown in Fig. V-9. I/V is written directly, without any algebraic manipulations, by using the superposition technique. It is easily shown that straightforward multiplication of the nine 2×2 matrices involves 2040 multiplications, and 36 additions, and results in an answer that contains 256 terms which can only be reduced to our expression after further algebraic maniupulations.

The frequency response of multicavity klystrons has been programmed on the analog computer of the Dynamic Analysis and Control Laboratory, M.I.T. The gain and phase characteristics of a four-cavity klystron (like the VA-87) and of a seven-cavity klystron are being evaluated.

A. Bers

2. Stagger-Tuning Experiments on Pulsed Klystrons

The small-signal gain-bandwidth characteristics of a stagger-tuned klystron were measured (measurements were made at Lincoln Laboratory) on a Varian Associates VA-87 four-cavity klystron which was designed for power outputs up to the one megawatt range. This tube has four identical, equally spaced, tunable cavities and a measured small-signal gain of 64 db with all cavities synchronously tuned. It was operated with the following characteristics:

Beam voltage,	95 KV	
Perveance,	1.8×10^{-6} amp/volt$^{3/2}$	
Pulsewidth,	1 μsec	
Distance between successive cavity gaps,	$0.148\ \lambda_q$	
(λ_q = wavelength corresponding to the reduced plasma frequency)		
Gap coupling coefficient,	0.765	
Gap transit angle,	1.6 radians	
Q and R shunt, including beam and circuit loading:	Q	R
Input cavity	70	8×10^3 ohms
Output cavity	40	5×10^3
Intermediate cavities	110	12.5×10^3

With the use of these parameters, the calculated value of the quantity K (defined by A. Bers, Section V-B.1), in terms of the normalized impedances, F_1 and F_2, of the first and second intermediate cavities, is

$$K = -j\ 553\ F_1F_2 + 28.1\ (F_1 + F_2) + j\ (0.4)$$

where $K = \frac{I}{V}\frac{Z_o}{\sin\theta}$, $F = \frac{1}{1 + jx}$, and $x = 2Q\frac{\omega - \omega_o}{\omega_o}$.

It would have been desirable to measure only the effect of the stagger tuning of the intermediate cavities, that is, the gain-bandwidth characteristics of $|K|^2$, since a klystron designed for broadband use would have input and output cavities with bandwidths comparable to that of $|K|^2$. Because of a mechanical failure of the tuning mechanism in the tube that was tested, the characteristics of the input cavity were not known with sufficient accuracy for the correction of this effect. The output cavity, which has a bandwidth more than twice that of the intermediate cavities, would have small effect over the band covered. Thus the curves in Fig. V-10 include the bandwidth reduction effect of the input and output cavities. However, they agree both in bandwidth and relative amplitude with curves obtained from computer solutions of the $|K|^2$

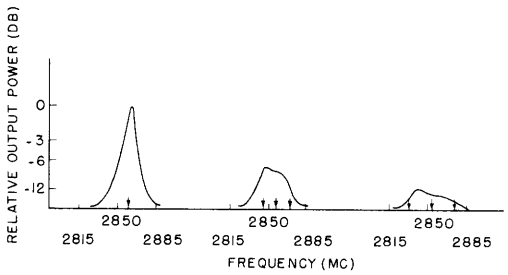

Fig. V-10. Small-signal frequency response of VA-87 four-cavity klystron amplifier. Arrows indicate tuning of intermediate cavities; first and last cavities are tuned to center frequency.

expression, indicating that, for the amount of detuning shown, the input and output cavities can be considered sufficiently broadband. (Analog computer solutions for this and other cases will be included in a future report.)

The curves (Fig. V-10) give the relative value of power to the output load versus frequency for: (a) all cavities tuned to a center frequency of 2856 mc; (b) intermediate cavities tuned to one-half bandwidth on opposite sides of the center frequency; and (c) intermediate cavities tuned to 3/4 bandwidth on opposite side. The resonant frequencies of each are indicated by arrows on the frequency axis.

Preparations are being made to obtain similar curves under large-signal conditions.

B. A. Highstrete

3. High-Perveance Cylindrical Electron Beams

The use of high-perveance tubular beams (see Quarterly Progress Report, Jan. 15, 1956, p. 51) in microwave tubes offers a number of advantages. As a matter of fact, such beams have already been successfully used in traveling-wave tubes and backward-wave oscillators. It seems probable that appreciable improvement in high-power klystrons could be obtained with Harris-flow beams. In this fashion, not only the higher perveance requirement would be fulfilled but also the main focusing solenoid(s) could be dispensed with. The need for an inner conductor can be satisfied by a "transparent" (nonsynchronous) helix. Such a helix will not couple to the beam at the operating frequency of the tube, and will couple very weakly to the cavities; but it should provide the necessary dc inner-drift tube potential. The advantages offered by a preliminary Harris-flow klystron design seem to justify further investigation of the associated problems.

C. Fried

C. FERRITES

1. Ferrite Resonance Isolator in Trough Waveguide

An investigation of resonance ferrite isolators in the new "trough" waveguide (1, 2, 3, 4) was undertaken. The waveguide has the cross section shown in Fig. V-11. It can be considered as a rectangular waveguide cut along the middle of one of the broad walls and bent across the middle of the other, whereupon the side walls are extended to prevent radiation from the structure.

The main advantages of this structure over the ordinary rectangular waveguide are the following: (a). Since even TE modes cannot exist here, it carries the TE_{10} mode in a frequency range of 3:1, instead of 2:1. (b). The open structure is more convenient for experimental work. (c). Transitions to coaxial lines are simpler, and it is believed that broadband operation is more easily obtainable (Fig. V-12).

For the TE_{10} mode, the cutoff wavelength is equal to four times the electrical height of the center fin. A good approximation (Fig. V-11) is

$$\frac{\lambda c}{2} = s + b \qquad (1)$$

For a waveguide with $s/2 = 2b = 7/8$ inch, the observed λc was 11.3 cm; but, from Eq. 1, λc should be 11.1 cm.

To utilize the entire 3:1 frequency band, the distance 2b between the side walls should be kept below one half of the next higher cutoff wavelength, since heavy radiation takes place at wavelengths shorter than 4b. [For the waveguide with $s/2 = 2b = 7/8$ inch, heavy radiation took place for all frequencies above 6.7 kmc and prevented the use of the upper part of the TE_{10} frequency range (2.7-8.1 kmc).] For practical purposes, the height of the side walls can be made three times that of the center fin.

It is easily recognized that there is a plane parallel to the bottom of the waveguide, in which the TE_{10} rf magnetic fields in the two parts are circularly polarized in the same sense as if they were seen from a direction perpendicular to the side walls. This indicates the possiblility of making ferrite resonance isolators by placing ferrite rods in or near that plane and magnetizing them, as shown in Fig. V-13.

The measurement apparatus is shown in Fig. V-14. The waveguide dimensions were: $s/2 = 2b = 7/8$ inch. The height of the side walls was 2 5/8 inches. The isolation was measured as the difference (in decibels) of the power level from the generator when the magnetic field was reversed, the probe position and the probe power being kept constant. The insertion or forward loss was measured by probing the fields on both sides of the ferrite. The ferrites were Ferramic 1331, for which the saturation magnetization ($4\pi M$) is approximately 2000 gauss, and the resonance line width (ΔH) is approximately 500 oersteds. The three ferrite-to-waveguide geometries shown in Fig. V-15 — all with the same cross-section area and length — were investigated. The ferrite dimensions

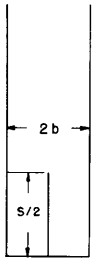

Fig. V-11. Cross section of trough waveguide.

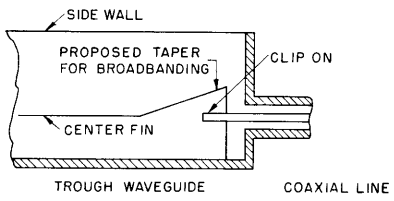

Fig. V-12. Coaxial line to trough waveguide transition.

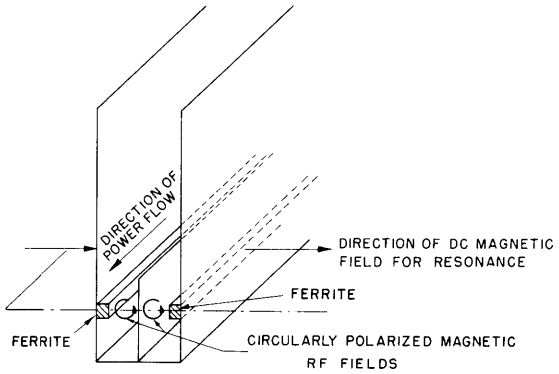

Fig. V-13. Principle of resonance isolator in trough waveguide.

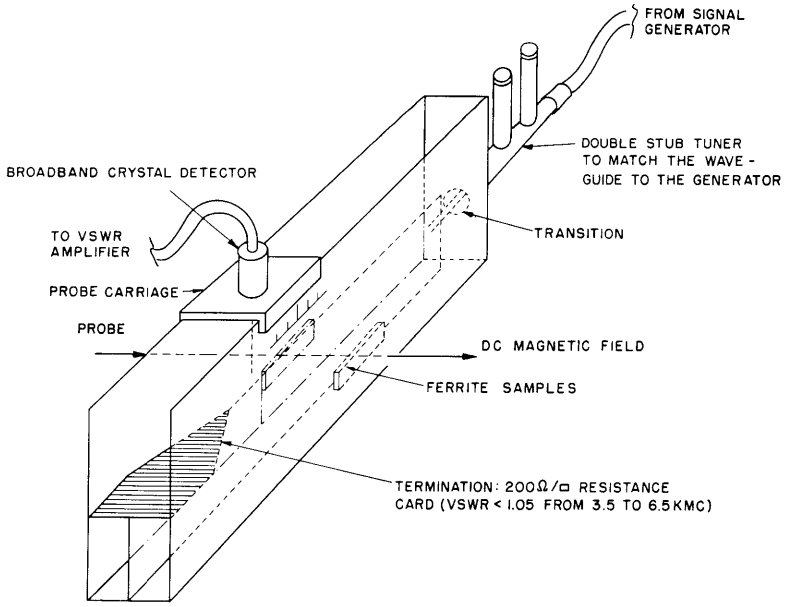

Fig. V-14. Section of experimental trough waveguide.

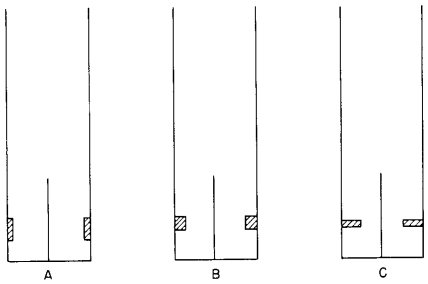

Fig. V-15. Ferrite-to-waveguide geometry.

were: in cases A and C (Fig. V-15), 2 1/2 × 1/4 × 1/16 inch; in case B, 2 1/2 × 1/8 × 1/8 inch.

To find the best combinations of resonant frequency and ferrite positions, the frequency dependence of the forward and reverse losses for different fixed positions of the ferrites was measured with the magnetic field set for resonance at each frequency. The results of these measurements of cases A and C are shown in Figs. V-16 and V-17. Similar measurements were made for case B. From Figs. V-16 and V-17, it can be seen that in going from A to C: (a) the losses increase, but the ratio of reverse to forward loss decreases; (b) the minimum of the forward losses becomes less flat; (c) the variation of forward loss with frequency increases; (d) the optimum value of x increases as the frequency decreases. The optimum positions are much nearer the bottom of the waveguide than the corresponding positions for circularly polarized fields in an empty waveguide. If we assume that the magnetic fields near the bottom of the trough are approximately the same as those for the equivalent rectangular waveguide, these positions are given by

$$\cos 2x' = 1 - \left(\frac{fc}{f}\right)^2 \qquad (2)$$

For the waveguide in question, fc, the cutoff frequency, is 2660 mc; thus, for 4500 mc, x' will be 36°; for 5250 mc, 30.5°; and for 5500 mc, 26°.

Figure V-18 shows the frequency dependence of the external dc magnetic field that is required for resonance. For the same applied field in cases A, B, and C (Fig. V-15), A will resonate at a low frequency, B at an intermediate frequency, and C at a high frequency. This is caused by the demagnetization, which increases from C to A, lowering the internal magnetic field in the ferrites and thus lowering the resonant frequency. Theoretically, it is accounted for by the Kittel equation.

Figures V-19 and V-20 show the frequency dependence of the forward and reverse losses for fixed magnetic fields and fixed optimum position of the ferrites. It is seen that the 3-db bandwidth is the same for cases A and C, but that A is better than C

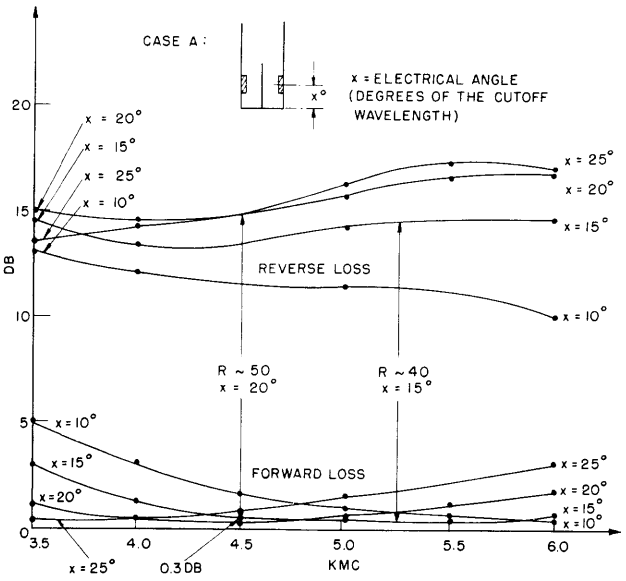

Fig. V-16. Frequency dependence of forward and reverse losses for fixed positions of ferrites (case A).

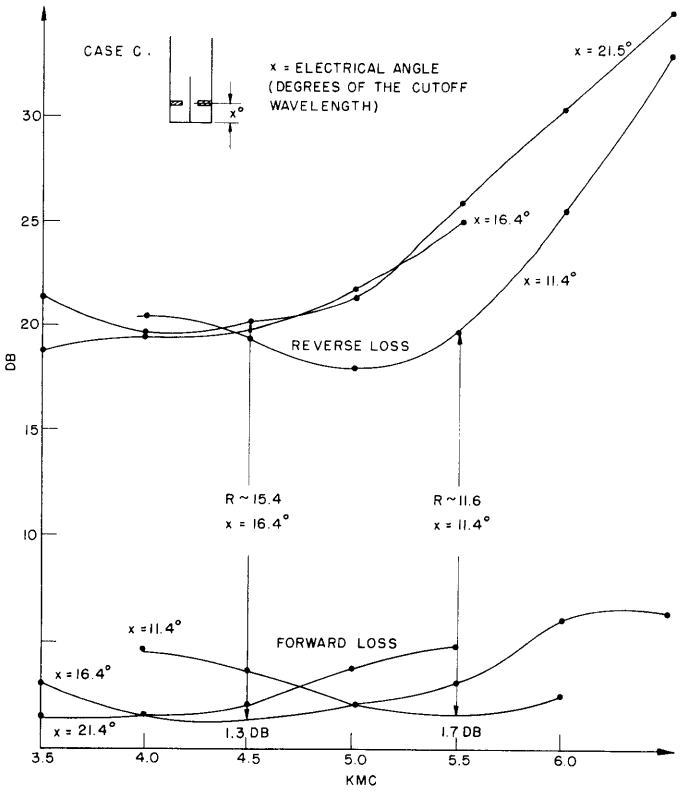

Fig. V-17. Frequency dependence of forward and reverse losses for fixed positions of ferrites (case C).

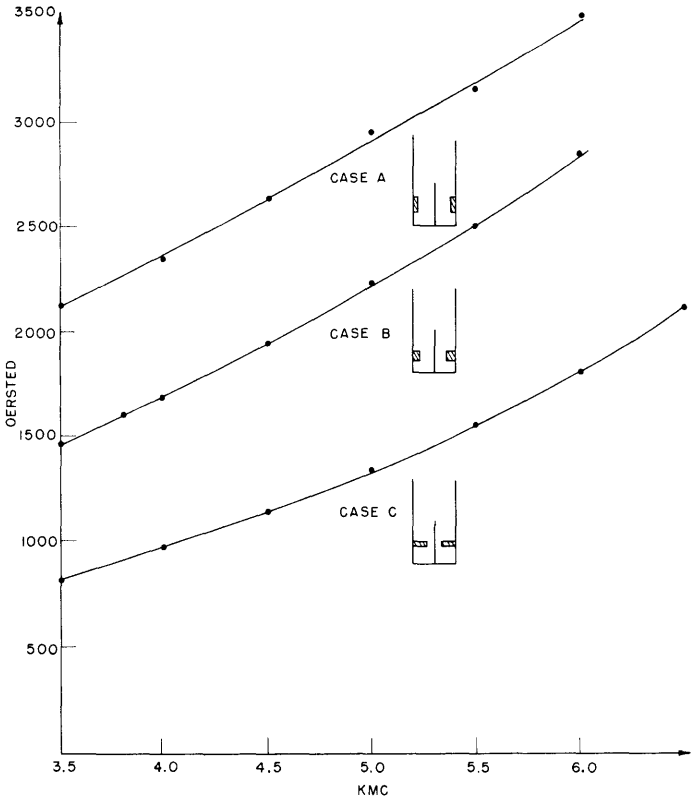

Fig. V-18. Frequency dependence of external dc magnetic field for resonance.

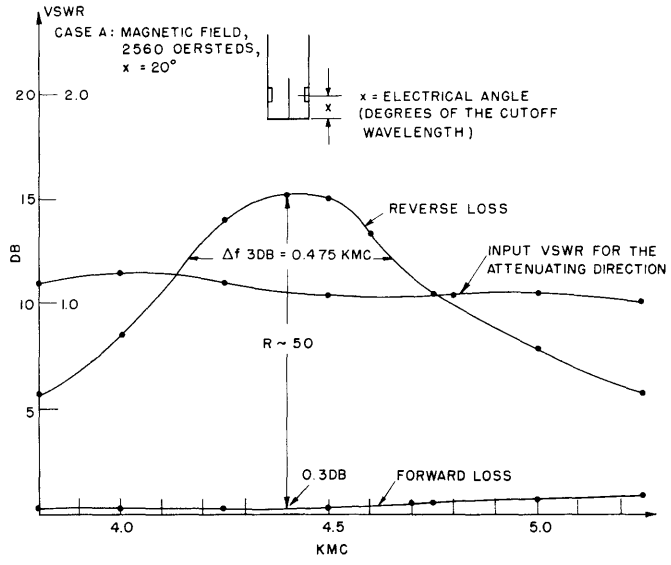

Fig. V-19. Frequency dependence of forward and reverse losses for fixed magnetic fields and fixed optimum position of the ferrites (case A).

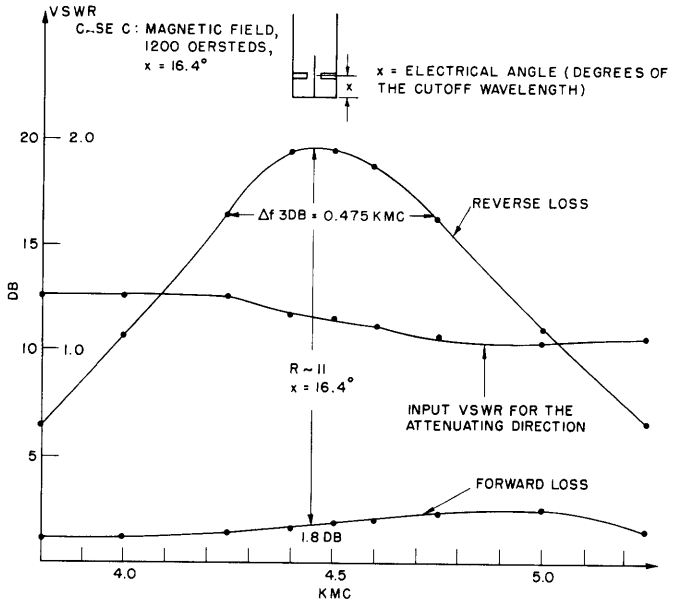

Fig. V-20. Frequency dependence of forward and reverse positions of the ferrites (case C).

with respect to the obtainable R. This superiority of A over C has also been recognized for rectangular waveguide isolators. Other advantages of A over C are:

a. The impedance match is better. This is attributable to less dielectric effect, as well as to the fact that the circularly polarized field outside the ends of the ferrites matches better than the circularly polarized fields inside the ferrite. In fact, it is not generally possible to have pure circularly polarized fields inside the ferrites for case C [see ref. 5, Eq. (32)].

b. Case A is better suited for high-power operation than C because arcing is less likely and the cooling conditions for the ferrites are better. Similar measurements were taken for case B; they show that the properties for this configuration are, on the average, similar to those for cases A and C.

It was expected that the rf magnetic fields near the bottom of the trough would be equal across the waveguide for the same height above the bottom, and thus the ferrites would act in the same way whether they were placed on the side walls or on the center fin. However, it was found for case A, that the 3-db bandwidth of the resonance curve was decreased from 11 per cent (Fig. V-19) to 9 per cent, and the ratio decreased from 50 to 27. It was also observed that the optimum position of the ferrites changes more rapidly with frequency at the center fin than at the side walls.

As stated in reference 5, the theoretical limit for the figure of merit – the ratio of reverse to forward loss – is given by

$$R_{max} \approx \left(\frac{4Hr}{\Delta Hr}\right)^2 \qquad (3)$$

Hr is the internal dc resonance field equal to f/γ, where f is the frequency in mc, and γ (the gyromagnetic ratio) is 2.8 mc/oersted. Equation 3 is based on the assumption that the rf magnetic fields are uniform over the cross section of the ferrites. For Ferramic 1331, for which ΔH is 500 oersteds, and for a frequency of 4500 mc, we find

$$R_{max} \approx \left(\frac{4 \times 4500}{2.8 \times 500}\right)^2 = 166$$

Compared with this value, an R of 50 seems to be poor. If, however, we consider the ratio of approximately 70, recently reported (ref. 5, p. 27, and related references) for a flat slab against the broad wall of a rectangular waveguide operating at 9280 mc (in which case Eq. 3 would give $R_{max} \sim 700$), the result seems better. Ratios nearer the theoretical limit were obtained by dielectric loading of the ferrites. The best result so far was obtained by G. S. Heller. At a frequency of 1300 mc, he obtained $R \sim 15$, where $R_{max} \sim 25$.

The help and advice of Dr. G. S. Heller, of Lincoln Laboratory, M.I.T., is gratefully acknowledged.

E. V. Sorensen

References

1. Symposium on microwave strip circuits, Trans. IRE, PGMTT, vol. MTT-3, No. 2 (March 1955).
2. N. Karas and W. Rotman, Some new microwave antenna designs based on the trough waveguide, IRE Convention Record, Part I, 1956, p. 230.
3. W. Rotman and N. Karas, Some further experimental results on the trough waveguide, Antenna Laboratory, Air Force Cambridge Research Center, March 1956 (Unpublished notes).
4. Proc. IRE 44, 2A (Aug. 1956).
5. B. Lax, Group Report M35-59, Lincoln Laboratory, M.I.T., March 14, 1956.